# Proposal of Multi-rate Controller for Vehicle body Slip Angle Based on Real-time Lane Detection

**Yafei Wang[1], Kanghyun Nam[1], Hiroshi Fujimoto[2] and Yoichi Hori[2]**
**The University of Tokyo, Japan**

[1]Department of Electrical Engineering, The University of Tokyo, Tokyo, 113-0033, Japan
[2]Department of Advanced Energy, The University of Tokyo, Chiba, 227-8561, Japan
Phone: (81) 04-7136-3873
Fax: (81) 04-7136-3847
E-mail: [1]{wang, nam}@hori.k.u-tokyo.ac.jp, [2]{fujimoto, hori}@k.u-tokyo.ac.jp

Body slip angle is considered as one of the key enablers for vehicle stability control, and it is desirable that the body slip angle can track reference in real-time. Therefore, on-line knowledge of the vehicle body slip angle is indispensible. However, existing products for body slip angle measurement are too expensive to be practically utilized. Thus, estimator is often designed to obtain the body slip angle for control purpose. As traditional models for body slip angle suffer from uncertainties such as cornering stiffness, this paper proposed a new model that combines bicycle model and vision model for estimation accuracy improvement. Moreover, to solve the sampling time mismatch issue between bicycle model and vision model, a multi-rate Kalman filter is designed in this paper. Finally, a two-degree-of-freedom (2DOF) controller is implemented for the desired body slip angle tracking with the multi-rate Kalman filter.

Topics / Vehicle Dynamics, Modeling and Simulation; Sensors and Actuators; Active & Passive Safety Systems

## 1. INTRODUCTION

Body slip angle is defined as the angle of the velocity vector measured from the vehicle's longitudinal axis [1], and it is one of the most important information for vehicle motion control systems. Due to the high complexity of vehicle dynamics, the response of body slip angle can become different from the driver's intention. Therefore, it is desirable to implement a control system that can manage the body slip angle so as not to exert pressure on the drivers. Nevertheless, in practice, off-the-shelf devices such as non-contact optical sensor are rarely employed for body slip angle measurement due to their high costs. Thus, methods for vehicle body slip angle estimation have been extensively studied during the last few decades. Based on the models used, estimation methods can be divided into two groups, i.e., kinematic model-based and dynamic model-based methods. Kinematic model-based method does not consider vehicle dynamics and therefore is insensitive to model parameter uncertainties; however, it suffers from sensor noise and drift. Based on the vehicle dynamics utilized, dynamic model-based method can be further divided into linear model-based and nonlinear model-based methods. Linear bicycle model-based observe is simple, but is sensitive to model uncertainties [2]. Nonlinear observer is more robust compared with the linear one, but it is very complex and requires high performance hardware. Considering the above mentioned backgrounds, a linear dynamic model-based observer that is robust against vehicle model uncertainties is desirable.

On the other hand, look-ahead cameras are becoming more and more popular in vehicles. In [3-4], it is found that, by detecting lane markers of the road and calculating the relative position of the vehicle to the lane, a vision model can be constructed based on simple geometry and thus contains much fewer uncertainties compared with the vehicle bicycle model. Moreover, the vision model can be combined with the traditional vehicle model, and therefore increase the observer's design freedom as well as the estimation accuracy [3]. In this study, by utilizing the estimated body slip angle as feedback, a two-degree-of-freedom controller is constructed for reference body slip angle tracking. However, two issues have to be handled due to the slow sampling rate of vision system. From the viewpoint of estimation, normal vision system and other kinds of onboard sensors are updated at different sampling rates, and thus can not be fused directly. From the viewpoint of control, with the electrification of vehicles, the sampling rate of actuators (such as in-wheel-motors) is higher than that of traditional vehicles, and therefore requires high speed feedback. The sampling sequence of the system is illustrated in Fig. 1.

## 2. SYSTEM MODELLING AND PROBLEM STATEMENT

In this section, a combined vehicle and vision model is introduced followed with further discussion of the problems.

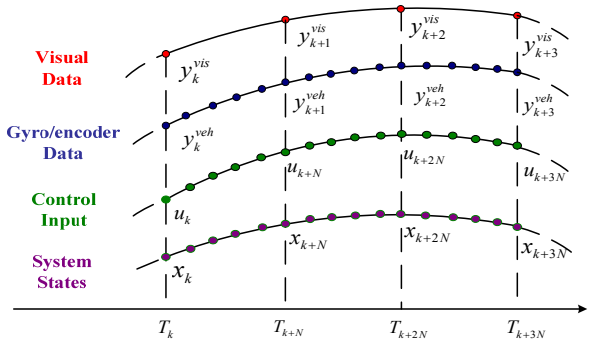


Fig. 1 System sampling time sequence

### 2.1 Vehicle Bicycle Model

Vehicle dynamics is non-linear in reality, and it is difficult to describe vehicle motion precisely. Although there are complex models that can describe the vehicle plant precisely, from the perspective of implementation, simple linear model is preferable. Vehicle bicycle model is widely used in vehicle state estimation and motion control systems. This model is illustrated in Fig. 2, and the governing equations are given in (1).

$$m \cdot V_x \cdot (\dot{\beta} + \gamma) = 2 \cdot C_f \cdot (\delta_f - \frac{l_f}{V_x}\gamma - \beta) + 2 \cdot C_r \cdot (\frac{l_r}{V_x}\gamma - \beta)$$
$$I \cdot \dot{\gamma} = 2 \cdot l_f \cdot C_f (\delta_f - \frac{l_f}{V_x}\gamma - \beta) - 2 \cdot l_r \cdot C_r (\frac{l_r}{V_x}\gamma - \beta) \qquad (1)$$

where $\beta$ and $\gamma$ are body slip angle and yaw rate at vehicle's CoG (center of gravity), respectively, $\delta_f$ is steering angle, $V_x$ is vehicle's longitudinal speed, $m$ is vehicle mass, $N_z$ is the yaw moment generated by the differential torque of rear wheels, $I$ is the moment of inertial about yaw axis, $C_f$ and $C_r$ are the cornering stiffness of the front and rear wheels, respectively, $l_f$ and $l_r$ are the distance from CoG to front and rear wheels, respectively.

### 2.2 Vision System Model

As can be seen, the bicycle model is independent of road reference. On the other hand, vision model is based on the geometric relationships between vehicle and lane/road together. Vision model is also shown in Fig. 2, and the gray borders are lane makers. $l_{pre}$ is a fixed preview distance need to be calibrated beforehand.

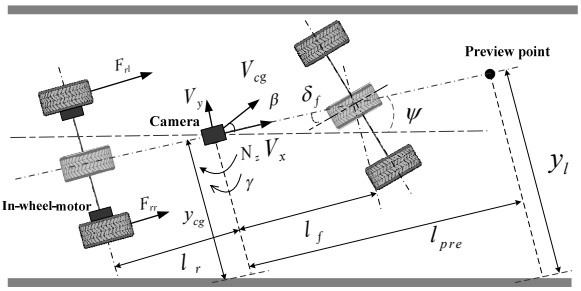


Fig. 2 Combined vehicle and vision model

In this model, it is assumed that the vehicle travels along a straight road with clear lane markers and the camera that equipped in the CoG (center of gravity) of the vehicle can detect the lane markers in real time. The lane function can be obtained in the coordinate with camera/vehicle as origin, and then, lateral distance offset $y_l$ at the preview point, as well as the heading angle $\psi$ can be calculated. $y_{cg}$ is the lateral offset at vehicle CoG.

To derive vision model, $\psi$ and $\beta$ are assumed to be small, and the governing equation can be geometrically obtained as (2). Heading angle $\psi$ can be simply modeled as integration of yaw rate as (3).

$$\dot{y}_l = V_x \cdot \beta + l_{pre} \cdot \gamma + V_x \cdot \psi \qquad (2)$$
$$\dot{\psi} = \gamma \qquad (3)$$

From (2), it can be known that, the derivative of offset at the preview point, i.e., lateral speed at that point, comprises three parts: the lateral speed of CoG, the components of yaw rate, and the component of longitudinal speed (resulted from vehicle heading angle).

### 2.3 Combined System Model

By combining (1) - (3) together, a new model can be given in continuous state space form as (4). In the system vector, the first two states are modeled by bicycle model and the latter two are modeled by the visual model. Obviously, the vision model is much simpler than the bicycle one. In the combined model, available system outputs are yaw rate, vehicle heading angle and lateral offset with reference to the lane at the preview point. The control input is the front steering and the differential torque generated by rear wheels.

$$\dot{x} = A \cdot x + B \cdot u + w$$
$$y = C \cdot x + v \qquad (4)$$

where

$$x = \begin{bmatrix} \beta & \gamma & \psi & y_l \end{bmatrix}^T, \quad u = \begin{bmatrix} \delta_f & N_z \end{bmatrix}^T, \quad y = \begin{bmatrix} \gamma & \psi & y_l \end{bmatrix}^T,$$

$$A = \begin{bmatrix} -\frac{2(c_f + c_r)}{m V_x} & -1 - \frac{2(c_f l_f - c_r l_r)}{m V_x^2} & 0 & 0 \\ -\frac{2(c_f l_f - c_r l_r)}{I} & -\frac{2(c_f l_f^2 + c_r l_r^2)}{I V_x} & 0 & 0 \\ 0 & 1 & 0 & 0 \\ V_x & l_{pre} & V_x & 0 \end{bmatrix},$$

$$B = \begin{bmatrix} \frac{2c_f}{m V_x} & \frac{2c_f l_f}{I} & 0 & 0 \\ 0 & \frac{1}{I} & 0 & 0 \end{bmatrix}^T, \quad C = \begin{bmatrix} 0 & 1 & 0 & 0 \\ 0 & 0 & 1 & 0 \\ 0 & 0 & 0 & 1 \end{bmatrix}.$$

### 2.4 Multi-rate Issue of the Combined Model for Estimation and Control

The combined system model has four states with three of them available from gyro sensor and image processing program, and it should be noted that the measurements from vehicle and vision models are sampled at different rates. For the vehicle model, the measurement is yaw rate that comes from gyro sensor, and it is updated every 1 ms in this study. For the vision model, the measured information was obtained from onboard vision system with an updating rate of 30 Hz. The illustration can be seen from Fig. 1. Therefore, data from vision system and from other onboard sensors cannot be fused directly because of sampling mismatch. Then, as stated in [3], two solutions can be employed, namely, single-rate and multi-rate estimation method. The single-rate estimator reduces the overall sampling rate to fit the slowest device (camera in this study), and the multi-rate estimator sets the system sampling time to 1 ms and can update the system states at 1 kHz. After obtaining the desired vehicle state, controller can be constructed with the estimated result as feedback. Nowadays, with the electrification of vehicles, actuators for motion control can also be motors [5]. In this research, an electric vehicle with in-wheel-motors (IWMs) is utilized, and the sampling time of IWMs is 1 ms. If feedback from the above mentioned single-rate estimator is utilized, the sampling time of the control input and output can not be consistent; the sampling time of the control input therefore has to be adapted to the control input which decrease the system stability margin. On the other hand, if information from multi-rate observer is employed, the system's open loop stability margin can be increased accordingly [6].

## 3. EXPERIMENTAL SETUPS

The experiment vehicle used in this research is an in-wheel-motor EV as in Fig. 3 (a). The prototype is COMS produced by Toyota Auto Body, and it was reengineered by our lab for capacitor research and motion control [7].

Fig. 4 briefly demonstrates the sensors and controller configurations of this vehicle. The vehicle controller is a PC104 embedded computer with ART-Linux operation system, and the program is configured to run at the speed of one millisecond per cycle. In addition to the central computer, four A/D converters and two counter boards are equipped for sensor signal reading. An IMU that measures lateral acceleration and yaw rate is installed in the vehicle CoG, and the signals are read by the A/D boards; steering angle and wheel speed encoders (installed in the non-driven wheel for vehicle speed measurement) are also equipped to send data to the counter board. To verify the effectiveness of estimation results, a non-contact optical sensor S-400 made by Corrsys-Datron is also equipped for body slip angle acquisition. Since this sensor is installed in front of the

(a)

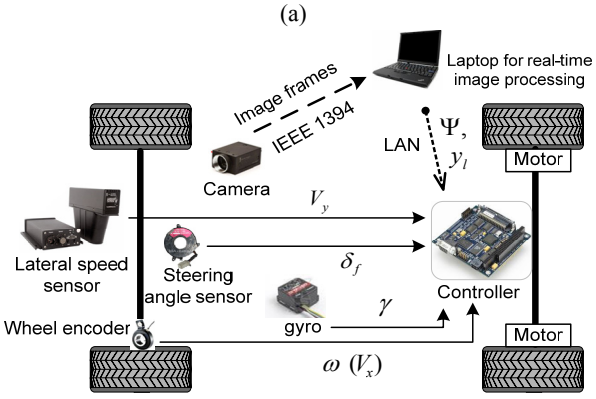


(b)

Fig. 3 (a) Experimental vehicle COMS, (b) Sensor configuration of COMS

vehicle, the measurements are compensated with yaw rate to get the value at vehicle CoG. The vision system includes a camera and an image processing laptop. The camera used is a monocular one produced by Point Grey, and it is installed on the top of the vehicle with a preview distance of 5.135 m. The frame rate of the camera is set to 30 fps.

Images captured by the camera are grasped by a CARDBUS frame grabber and processed by a laptop with image processing algorithms in Linux environment. The image processing time varies from 8 ms to 25 ms depending on the CPU load and the incoming images. To make the outputs from image processing program constant, a delay function is implemented. The final outputs from vision system are the estimated ψ and yl. The two values are sent to vehicle controller via LAN cable using UDP protocol. The data transmission time can be neglected.

## 4. LANE DETECTION BASED ON REAL-TIME IMAGE PROCESSING

To fuse vision information with signals from other onboard sensors, real-time image processing is required. Image processing in this research generally consists of two parts: coordinate mapping and images processing of the mapped image as described below [3, 8-9].

### 4.1 Coordinate Mapping.

Camera can map the 3-D world onto its 2-D image view; however, this kind of mapping loses important

information such as depth, which is why many studies use stereo camera instead of monocular one. For the application of lane detection and location, since common roads can be simplified as planar, a monocular camera is fairly enough to correlate pixels of the image with real roads.

Fig. 4 shows the geometric relationships among pinhole camera model, image plane and road plane. In Fig. 4, $h$ is height of camera, $f$ is focal length, $\theta$ is camera tilting angle, $\alpha_v$ and $\alpha_u$ are the angle of view in vertical and horizontal axis of image planes, respectively. To find the mapping matrix from image coordinate to road coordinate, one typical method is to calibrate the camera model which is composed of both intrinsic and extrinsic parameters. While this method needs complex calibration, another more straightforward method can get road coordinates from image pixel positions by deriving functions based on geometric relationships [10].

Given any pixel ($u_{pixel}$, $v_{pixel}$) in the image plane, its projection on the road plane is given as ($x$, $y$). Assuming the resolution of image is $m$ by $n$, the mapping between road coordinates and pixel coordinates is shown in equation (5).

$$v_{pixel} = \frac{m-1}{2} \cdot \left(1 + \frac{h - x \cdot \tan\theta}{h \cdot \tan\theta + x} \cdot \cot\alpha_v\right) + 1$$
$$u_{pixel} = \frac{n-1}{2} \cdot \left(1 - \frac{y}{h \cdot \sin\theta + x \cdot \cos\theta} \cdot \cot\alpha_u\right) + 1 \qquad (5)$$

In the vision system used in our experiment, the parameters in (5) are given as: (m, n) = (480, 640); $\alpha_v$ = 12.4°; $\alpha_u$ = 16.6°; $h$ = 1.65 m; $\theta$ = 8°. From (7), it can be noted that the row of pixel coordinates only has relationship with $x$ coordinates of the road plane, and the column of pixel coordinate correlates with both $x$ and $y$ coordinate of road plane. After pixel mapping, the generated image represents a bird-eye view of the road; from this bird view, the distance information of the vehicle to the lane can be known precisely, and can be used for position measurement.

### 4.2 Lane Detection and Location.

This part consists of two steps: the first step is to lane extraction from the background, and the second one is lane position locating. The final results are shown in Fig. 4.

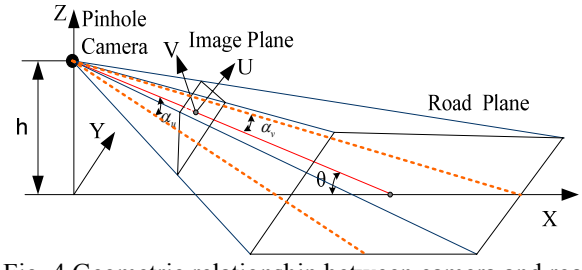


Fig. 4 Geometric relationship between camera and road

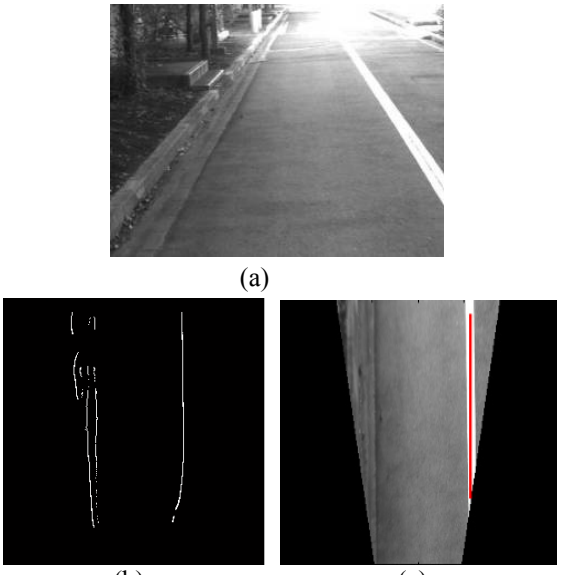

(a) (b) (c)

Fig. 5 Image processing result. (a) Original image, (b) Mapped and binarized image, (c) Lane locating result.

To detect the lane, Laplacian of Gaussian (LoG) method is utilized. LoG gives zero to the uniform region of the image; wherever a change occurs, the LoG will give a positive response on the darker side and a negative response on the lighter side, and hence the lane can be extracted. Although white lane marker can be extracted from image using the methods outlined above, the positions of white pixels are still unknown. In this study, RANdom SAmple Consensus (RANSAC) algorithm proposed by [11] is adopted to give the solution. This is a re-sampling technique that gives solutions by using the minimum number of required data required for model estimation. Unlike conventional sampling techniques that use as much data as possible to obtain an initial solution, RANSAC randomly selects a smallest data set and solves for the results; and then finds how many points in total fit the model within a given tolerance; if the fitting ratio is large enough, it ends with success, otherwise will proceed to prune outliers [11].

## 5. MULTI-RATE CONTROLLER FOR BODY SLIP ANGLE MANIPULATION

As body slip angle is not readily available as introduced before, it is first estimated with a multi-rate Kalman filter and is then given to the 2DOF controller as feedback.

### 5.1 Kalman Filter Based $\beta$ Estimation

To design the Kalman filter for real-time implementation, (4) has to be discretized to (6), where $T_s$ is the sampling time. Considering the multi-rate issues stated in section 2.4, $T_s$ is set to 1 ms. Detailed design of the multi-rate estimator can be found in [3].

$$x(k+1) = A_d(k)\cdot x(k) + B_d(k)\cdot u(k) + w(k)$$
$$y(k) = C_d(k)\cdot x(k) + v(k) \qquad (6)$$

where

$$A_d(k) = e^{A\cdot Ts}, \quad B_d(k) = \int_0^{Ts} e^{A\cdot\tau}\cdot B d\tau,$$
$$C_d(k) = C.$$

### 5.2 Design of 2DOF Controller

During real driving conditions, the body slip angle's response may not be able to follow the driver's control input. Therefore, it is desirable to implement a control system that can manipulate the body slip angle to a desired value without giving stress to the driver. In this study, the differential torque of left and right wheels can be used as control input. The overall control structure is shown in Fig. 6.

First of all, from the vehicle dynamics equation (1), the reference body slip angle can be calculated as (7) by assuming a steady state response is desired, where A is the stability factor given in (8).

$$\beta^* = G_{\delta_f}^{\beta\,*}\cdot\delta_f = \frac{1-\frac{ml_fV_x^2}{2l_rC_r}}{1+AV_x^2}\cdot\frac{l_r}{l}\cdot\delta_f \qquad (7)$$

$$A = -\frac{m}{2l^2}\cdot\frac{l_fC_f - l_rC_r}{C_fC_r} \qquad (8)$$

Then, a 2DOF controller is employed here for reference tracking and it consists two parts, namely, feed-forward and feedback controllers. Feed-forward controller is usually designed using the inversed system dynamics [12]. Here, the feed-forward controller therefore is calculated as (9) based on the system dynamics (10).

$$C_{FF} = \left(G_{N_z}^{\beta}\right)^{-1} \qquad (9)$$

$$G_{N_z}^{\beta} = -\frac{mV_x^2 + 2\left(l_fC_f - l_rC_r\right)}{4C_fC_rl^2\left(1+AV_x^2\right)} \qquad (10)$$

A feedback controller is necessary for system stabilization and disturbance rejection. The estimated $\beta$ is utilized as feedback signal and a PI controller is designed based on pole-placement. The feed-forward and feedback controller together generate the yaw moment for $\beta^*$ tracking.

After obtaining the desired yaw moment, the torque distribution law (TDL) needs to be considered. As introduced before, the rear wheels are utilized as actuators and they can be independently controlled to generate positive and negative torques. A simple TDL can be defined as (11):

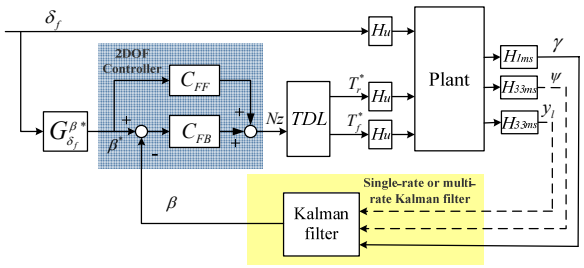


Fig. 6 Controller structure with β estimator.

$$T_r^* = \frac{m\cdot r\cdot a_x}{2} - \frac{2\cdot r\cdot N_z}{d_r}$$
$$T_l^* = \frac{m\cdot r\cdot a_x}{2} + \frac{2\cdot r\cdot N_z}{d_r} \qquad (11)$$

where $a_x$ is the acceleration rate and $N_z$ is the yaw moment to be distributed.

## 6. SIMULATION AND EXPERIMENTAL RESULTS

The performance of the multi-rate Kalman filter can be found in [3]. In this section, the controller's performance is verified in both simulation and experiment.

### 6.1 Simulation

With the proposed multi-rate Kalman filters, the performance of the body slip angle controller is verified in simulation. In this simulation, the vehicle is assumed to run at the speed of 30 km/h, and a sine steering input is given. As stated before, the open-loop response of the body slip angle may not be the same with the desired value, and this can be seen from the blue dotted and the green curves in Fig. 7. On the other hand, with the proposed controller, the body slip angle can track the desired value as shown by the red line in Fig. 7.

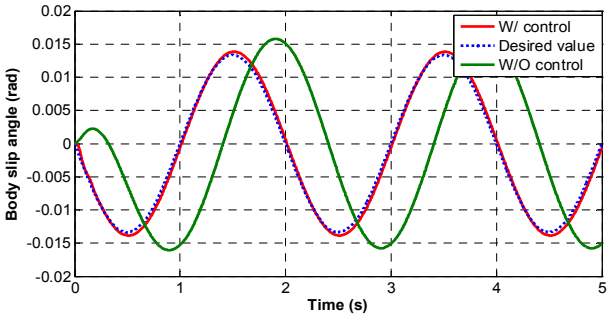


Fig. 7. Simulation comparison of w/ and w/o control.

### 6.2 Experiment

Then, the 2DOF controller with the multi-rate Kalman filters is implemented in the experimental vehicle introduced in section 3. The vehicle is given a sine steering input, and IWMs are used to generate differential torque to control the vehicle body slip angle for reference tracking in real-time. In Fig. 8 (a), the

steering input from the driver is shown, and the differential torque calculated from the 2DOF is given in Fig. 8 (b). In Fig. 8 (c), as can be observed, the body slip angle response can follow the reference very well with the assist of differential torque.

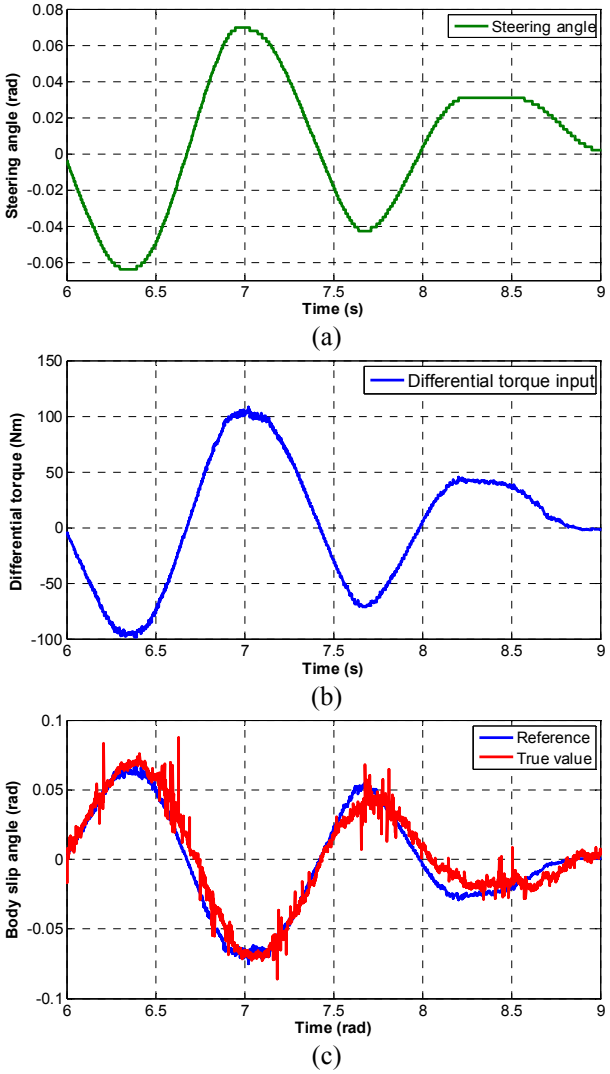


Fig. 8. Experimental results. (a) Steering input, (b) Generated differential torque, (c) The reference β following performance with control.

## 7. CONCLUSION AND FURTURE WORKS

In this paper, first of all, a combined vehicle and visual model was derived, and the multi-rate issues was explained; then, the experimental setups and the image processing techniques were introduced; and then, multi-rate Kalman filter that can be updated every 1 ms as well as the 2DOF controller were designed; finally, simulations and experiments were conducted to verify the proposed controllers with the multi-rate estimators. The further step of this research is to expand vision system to other vehicle motion estimation and control applications, for example, enhanced lane keeping control, roll angle estimation and control and so on.

## REFERENCES

[1] David Crolla, "Automotive Engineering! Powertrain, Chassis System and Vehicle Body", Elsevier, 2009, pp. 519-524.
[2] Y. Aoki, T. Uchida and Y. Hori, "Experimental Demonstration of Body Slip Angle Control based on a Novel Linear Observer for Electric Vehicle," IECON 2005, pp.2620-2625.
[3] Y. Wang, P. Kotchapansompote, B.M. Nguyen, H. Fujimoto, Y. Hori, "Vision-based Vehicle Body Slip Angle Estimation with Multi-rate Kalman Filter considering Time Delay," IEEE ISIE'12, Hangzhou, China, 2012.
[4] J. Hsu, M. Tomizuka, "Analyses of vision-based lateral control for automated highway system," Vehicle system dynamics, Vol. 30, pp. 345-373, 1998.
[5] Y. Hori, "Future Vehicle driven by Electricity and Control -Research on 4 Wheel Motored 'UOT March II'," IEEE Trans. Ind. Electron., vol.51, no.5, pp.954-962, Oct. 2004.
[6] H. Fujimoto and Y. Hori, "Visual servoing based on multirate sampling control," in IEEE Int. Conf. Robotics and Automation, 2001.
[7] K. Kawashima, T. Uchida, and Y. Hori, "Manufacturing of Small Electric Vehicle driven only by Electric Double Layer Capacitors for Easy Experiment of Vehicle Motion Control," Electric Vehicle Symposium 21, 2005.4.
[8] M. Bertozzi and A. Broggi, "GOLD: a Parallel Real-Time Stereo Vision System for Generic Obstacle and Lane Detection," IEEE Trans. Image Process, pp. 62-81, Jan. 1998.
[9] Joel C. McCall and Mohan M. Trivedi, "Video Based Lane Estimation and Tracking for Driver Assistance: Survey, System, and Evaluation," IEEE Trans. Intell. Transp. Syst., vol.7, pp.20-37, 2006.
[10] Muad, A.M. Hussain, A. Samad, S.A. Mustaffa, M.M. Majlis, B.Y., "Implementation of inverse perspective mapping algorithm for the development of an automatic lane tracking system," TENCON 2004, vol. 1, pp. 207-210, 2004.
[11] M.A. Fischler and R.C. Bolles, "Random sample consensus: A paradigm for model fitting with applications to image analysis and automated cartography," Commu. of the ACM, Vol. 24, pp. 381-395, June 1981.
[12] R. Minaka and Y. Hori, "Two Degree of Freedom Control of Active Front Steering System using Planetary Gear," AVEC 2010, Loughborough, UK.